Photochemical & Photobiological Sciences

Accepted Manuscript

This is an *Accepted Manuscript*, which has been through the Royal Society of Chemistry peer review process and has been accepted for publication.

Accepted Manuscripts are published online shortly after acceptance, before technical editing, formatting and proof reading. Using this free service, authors can make their results available to the community, in citable form, before we publish the edited article. We will replace this *Accepted Manuscript* with the edited and formatted *Advance Article* as soon as it is available.

You can find more information about *Accepted Manuscripts* in the Information for Authors.

Please note that technical editing may introduce minor changes to the text and/or graphics, which may alter content. The journal's standard Terms & Conditions and the Ethical guidelines still apply. In no event shall the Royal Society of Chemistry be held responsible for any errors or omissions in this *Accepted Manuscript* or any consequences arising from the use of any information it contains.

ROYAL SOCIETY OF CHEMISTRY

www.rsc.org/pps

Journal Name

RSCPublishing

ARTICLE

Evaluation of the Charge Transfer Efficiency of Organic Thin-Film Photovoltaic Devices Fabricated Using Photoprecursor Approach

Cite this: DOI: 10.1039/x0xx00000x

Received 00th January 2012,
Accepted 00th January 2012

DOI: 10.1039/x0xx00000x

www.rsc.org/

Sadahiro Masuo[a,d], Wataru Sato[a], Yuji Yamaguchi[b,d], Mitsuharu Suzuki[c,d], Ken-ichi Nakayama[b,d], Hiroko Yamada[c,d]

Recently, a unique 'photoprecursor approach' was reported as a new option to fabricate p-i-n triple-layer organic photovoltaic device (OPV) through solution processes. By fabricating the p-i-n architectures using two kinds of photoprecursors and a [6,6]-phenyl C_{71} butyric acid methyl ester ($PC_{71}BM$) as donor and acceptor, the p-i-n OPVs afforded higher photovoltaic efficiency than the corresponding p-n devices and i-devices, while the photovoltaic efficiency of p-i-n OPVs depended on the photoprecursors. In this work, the charge transfer efficiency of the i-devices composed of the photoprecursors and $PC_{71}BM$ was investigated using high-sensitivity fluorescence microspectroscopy combined with a time-correlated single photon counting technique to elucidate the photovoltaic efficiency depending on the photoprecursors and the effects of the p-i-n architecture. The spatially resolved fluorescence images and fluorescence lifetime measurements clearly indicated that the compatibility of the photoprecursors with $PC_{71}BM$ influences on the charge transfer and the photovoltaic efficiencies. Although the charge transfer efficiency in the i-device was quite high, the photovoltaic efficiency of the i-device was much lower than that of p-i-n device. These results imply that the carrier generation and the carrier transportation efficiencies can be increased by fabricating the p-i-n architecture.

Introduction

Organic photovoltaic devices (OPVs) are an emerging technology with promising advantages, such as low cost, flexibility, light weight, transparency and large-area manufacturing compatibility.[1-13] A fundamental problem of organic materials is that carriers, such as excitons, electrons, and holes, tend to localize more in molecules than in inorganic semiconductor materials. Due to this tendency, the diffusion or hopping length of the carriers in organic materials is limited to a scale of nanometers. Therefore, the arrangement of the organic materials with nanometer-scale precision in the active layers of the OPVs is essential for constructing efficient photon-to-current energy conversion systems. In particular, the design of the donor–acceptor interface is of great importance to improve the device performance of OPVs. Recent studies have achieved a power conversion efficiency (PCE) of 8–12% in bulk-heterojunction (BHJ) OPVs.[14-16] In addition to the design of the active layer, the vertical composition profile of the active layer significantly affects the efficiency of charge-carrier generation and transportation.[17-19] The vertical composition profile, layer by layer deposition of different materials, can be done straightforwardly via vacuum evaporation, while solution processes are practically challenging because of dissolution of the lower layers during the deposition of the upper layer.

Recently, some of authors have reported a unique 'photoprecursor approach' as a new option for layer-by-layer preparation of multicomponent organic semiconducting films through solution processes.[20] In this approach, soluble photoprecursors, 2,7-bis(thiophen-2-yl)-5,10-dihydro-5,10-ethanoanthracene-12,13-dione (DTADK) and 2,6-bis(5'-(2-ethylhexyl)-(2,2'-bithiophen)-5-yl)-9,10-dihydro-9,10-ethanoanthracene-11,12-dione (EH-DBTADK) (Fig.1), were solution-deposited then photoconverted in situ to a poorly soluble organic semiconductor. This approach enables solution-processing of the p-i-n triple-layer architecture that has been suggested to be effective in obtaining efficient OPVs. Both p-i-n OPVs fabricated using DTADK and EH-DBTADK afforded higher photovoltaic efficiencies than the corresponding p-n devices (double-layer of p- and n-type materials) and BHJ devices (p:n composite layer; i-layer), while the photovoltaic efficiency of p-i-n OPV composed of EH-DBTADK was much higher than that of DTADK.[20]

The photocurrent generation of OPVs consists of the following processes: (i) generation of excitons by absorbing photons (A), (ii) exciton diffusion and charge transfer at the

interface (ED), (iii) charge separation by overcoming the charge recombination, i.e., the generation of holes and electrons at the interface (CS), and (iv) the collection of holes and electrons at the electrodes (CC). The external quantum efficiency (EQE) as a function of wavelength (λ) is given using the efficiencies (η) of these processes as follows: EQE(λ) = ηA(λ) × ηED(λ) × ηCS(λ) × ηCC(λ). The efficiencies of these various processes must be optimized to create OPVs with high PCE; a high PCE cannot be achieved if even one of these processes has a low efficiency.

In this work, we investigated the charge transfer efficiency (ηED) of the BHJ-OPVs (i-device) fabricated by DTADK and EH-DBTADK using a fluorescence microspectroscopy technique combined with the fluorescence lifetime and spectrum measurements to elucidate the difference of the photovoltaic efficiency depending on the photoprecursors and the effects of p-i-n architecture. To investigate the charge transfer in OPVs, spectroscopic studies such as the fluorescence quenching,[21-23] transient absorption spectroscopy,[24-27] and spatially resolved imaging techniques[28-32] have been used. We employed a high-sensitivity fluorescence microspectroscopy technique to evaluate the ηED with sub-micrometer spatial resolution in the device. Using fluorescence images observed from micrometer-sized areas of the BHJ-OPVs and the fluorescence lifetimes detected at focal points in the images using a confocal fluorescence microscope, the spatially resolved ηED in the device was estimated accurately without being affected by the thickness of the active layer, the concentrations of donor/acceptor molecules, or other parameters. The correlation between the obtained ηED and photovoltaic efficiency is discussed.

Experimental

Materials. The chemical structures of the photoprecursors, DTADK and EH-DBTADK, and their photoconversion reaction are shown in Fig. 1. DTADK and EH-DBTADK were synthesized according to the reported procedures.[20,33] The purities of these compounds were confirmed to be >99% by high performance liquid chromatography. [6,6]-phenyl C_{71} butyric acid methyl ester ($PC_{71}BM$, >99%) was purchased from Luminescence Technology Corp. and used as received. Other reagents and solvents were reagent grade purchased from commercial vendors and used without further purification.

Device fabrication and evaluation. PEDOT:PSS (CleviousTM AI4083, Heraeus) was spin-coated onto a clean ITO substrate. After baking in a vacuum at 120°C for 10 min, the substrate was transferred to a nitrogen-filled glove box (< 1 ppm O_2 and H_2O). A chloroform solution, in which the photoprecursor as a p-type material and $PC_{71}BM$ as a n-type material were dissolved at a weight ratio of 2:1 (10 mg mL^{-1}), was spin-coated at 800 rpm for 30 s. The photoprecursors in the mixed film were photoconverted into their parent acenes (DTADK into DTA, or EH-DBTADK into EH-DBTA) upon irradiation with a blue light-emitting diode (LED) lamp (wavelength: 470 nm, intensity: 200 $mWcm^{-2}$, Edmund Optics), and Ca and Al were evaporated as cathodes. The device was then encapsulated with a glass lid. As references, neat films of the parent acenes were prepared from a solution of the photoprecursors (5 mg mL^{-1}) without $PC_{71}BM$ in the same manner. The surface morphologies of the active layers in OPV devices and the neat film were evaluated by AFM measurement (NanoWizard@, JPK instruments). The photovoltaic performance was evaluated under AM 1.5G illumination with an intensity of 100 $mWcm^{-2}$ using a solar simulator system (CEP-2000, BUNKOUKEIKI). Details of the fabrication and evaluation of the devices were reported elsewhere.[20,34,35]

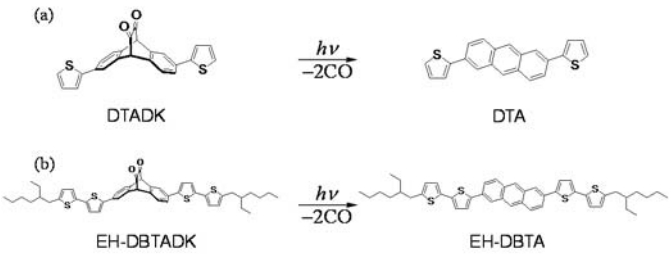

Fig. 1 Chemical structures of photoprecursors and their photoconversion to parent acenes.

Evaluation of charge transfer efficiency. The ηED of the prepared BHJ-OPVs was evaluated using a sample-scanning confocal microscope in combination with a picosecond-pulsed laser excitation (405 nm or 640 nm, 10 MHz, 100 ps FWHM, Picoquant). The fluorescence from the active layer of the OPV device was collected by an objective lens and passed through a confocal pinhole (100 μm) and suitable filters. To detect the fluorescence of the parent acenes, a 405 nm laser was used, and a long-pass filter and a short-pass filter were used to cut the excitation laser beam and fluorescence from $PC_{71}BM$, respectively. The fluorescence of $PC_{71}BM$ was detected using a 640 nm laser, and a long-pass filter was used to cut the excitation laser beam. The detected fluorescence was split into two paths and were detected using a spectrometer with a cooled CCD camera and an avalanche single-photon counting module (APD: SPCM-AQR-14, PerkinElmer). The signal from the APD was connected to a time-correlated single-photon counting board. The time-resolution of the lifetime measurement, i.e., the instrumental response function (IRF) of the system, was estimated by the deconvolution analysis of a fluorescence decay curve of erythrosine in water, which has a reported fluorescence lifetime of 87 ps.[36] The estimated FWHM of the IRF was approximately 300 ps. The fluorescence images, lifetime, and spectra of the BHJ-OPVs were measured simultaneously using this setup. Details can be found in Supplementary Information (SI). All measurements were performed at room temperature under ambient conditions.

Results and discussion

The photovoltaic performances of the BHJ-OPVs fabricated using the photoprecursors and $PC_{71}BM$ are summarized in Table 1. The short-circuit current (J_{SC}) of the EH-DBTA:$PC_{71}BM$ device (3.71 $mAcm^{-2}$) was significantly larger than that of the DTA:$PC_{71}BM$ device (2.38 $mAcm^{-2}$). The value of J_{SC} can be determined as the integration of EQE (λ) = ηA (λ) × ηED (λ) ×

ηCS (λ) × ηCC (λ), where ηED (λ) × ηCS (λ) × ηCC (λ) is the internal quantum yield (IQE). The EQE, IQE, and UV-Vis absorption spectra measured from the two OPVs are shown in Fig. 2. The EQE and IQE of EH-DBTA:$PC_{71}BM$ are larger than those of DTA:$PC_{71}BM$ over the entire wavelength region. Hence, the J_{SC} of EH-DBTA:$PC_{71}BM$ was larger than that of DTA:$PC_{71}BM$. In contrast, the open circuit voltage (V_{OC}) of the DTA:$PC_{71}BM$ device was larger than that of the EH-DBTA:$PC_{71}BM$ device (Table 1). The larger V_{OC} of the DTA:$PC_{71}BM$ device is attributed to the larger HOMO-LUMO band-gap of DTA (2.67 eV) compared to that of EH-DBTA (2.42 eV). Thus, the difference between PCEs became smaller, with values of 0.68 and 0.85 obtained from the DTA:$PC_{71}BM$ and EH-DBTA:$PC_{71}BM$ device, respectively. As noted above, the J_{SC} values of the two devices differed due to the difference in their IQEs. The IQE is determined by the ηED, ηCS, and ηCC. In the following discussion, the ηEDs in two OPVs will be evaluated using fluorescence microspectroscopy to establish the effect of the ηED on the J_{SC} value in each device.

First, the ηED in a BHJ-OPV fabricated using DTADK and $PC_{71}BM$ was investigated. The fluorescence images obtained from a 20 × 20 μm area in the OPV and DTA neat film are shown in Fig. 3. Figure 3 (a) corresponds to the fluorescence intensity distribution of DTA in the OPV observed by a 405 nm excitation. High- and low-intensity areas were both present across the device. The fluorescence intensity (I_f) is expressed as follows:

$$I_f = I_{ex}\alpha l \Phi_f \eta_{det} \qquad (1),$$

where I_{ex} is the excitation intensity, α is the absorption coefficient, l is the thickness of the sample (number of fluorescent molecules at the focal point), Φ_f is the fluorescence quantum yield, and η_{det} is the detection efficiency of the instrument. Φ_f can be expressed as follows:

$$\Phi_f = \frac{k_r}{k_r + k_{nr} + k_{ED}} \qquad (2),$$

where k_r and k_{nr} are the radiative and nonradiative decay rates, respectively, and k_{ED} is the charge transfer rate. When the fluorescence image was observed, I_{ex} and η_{det} were constant such that the heterogeneity of the fluorescence intensity was attributed to the difference in the thickness of the DTA layer and/or Φ_f which varies depending on k_{ED} assuming that k_r andk_{nr} are constant. Figure 3 (c) shows the fluorescence image of a DTA neat film observed by a 405 nm excitation (Note: the intensity-scale is different from that of BHJ-OPVs). This neat film showed much higher fluorescence intensity, and the heterogeneity of the fluorescence intensity was also observed in the neat film, which indicated that the DTA did not form a uniform film.

AFM measurements were conducted to evaluate the film structures of the active layer of the OPV and neat film. The obtained AFM images are shown in Fig. 4. Many broad peaks of several tens to a hundred nm in height were observed in the AFM images. The distance between the peaks was wider in the OPV device compared to that in the neat film due to the presence of $PC_{71}BM$ in the OPV device (vide infra). The fluorescence and AFM images indicated that DTA tended to aggregate because of

Table 1 Photovoltaic device performance of a BHJ-OPVs consisting of photoprecursors and $PC_{71}BM$.

	J_{SC}/mAcm^{-2}	V_{OC}/V	FF/%	PCE/%
DTA:$PC_{71}BM$	2.38	1.06	26.8	0.68
EH-DBTA:$PC_{71}BM$	3.71	0.78	29.4	0.85

J_{SC}: short circuit current, V_{OC}: open circuit current, FF: fill factor, PCE: power conversion efficiency

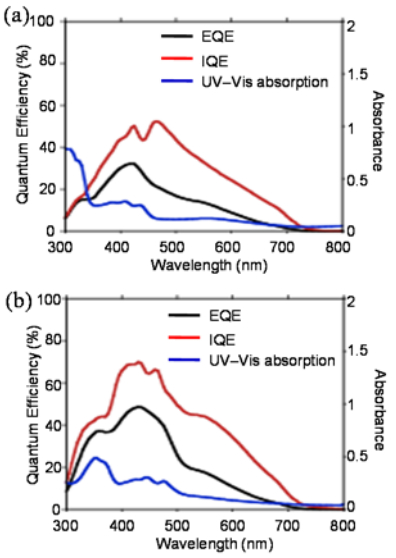

Fig. 2 EQE(λ) (black), IQE(λ) (red), and UV-Vis absorption spectra (blue) measured from the OPVs consisting of DTA:$PC_{71}BM$ (a) and EH-DBTA:$PC_{71}BM$ (b).

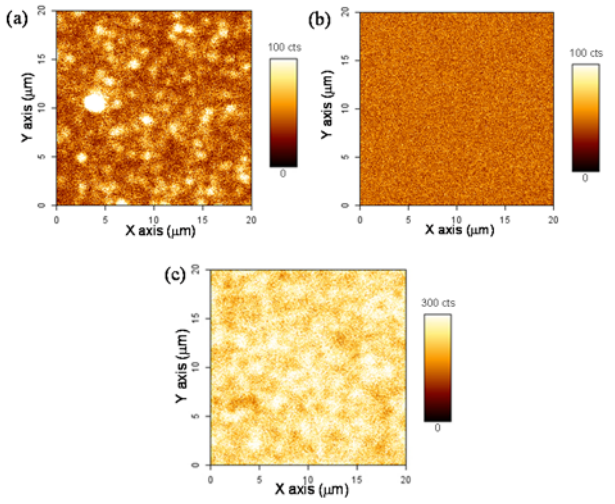

Fig. 3 Fluorescence images observed from a BHJ-OPV consisting of DTA and PC71BM (a, b) and from a DTA neat film (c). Images (a, c) were observed by a 405 nm excitation with a 56 W/cm^2 intensity, and image (b) was observed by a 640 nm excitation with a 4.5 kW/cm^2 intensity.

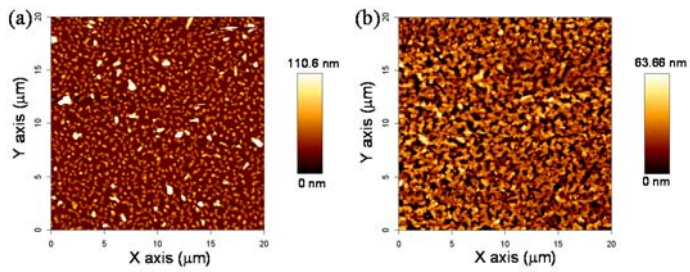

Fig. 4 AFM images obtained from the OPV consisting of DTA and $PC_{71}BM$ (a) and a DTA neat film (b).

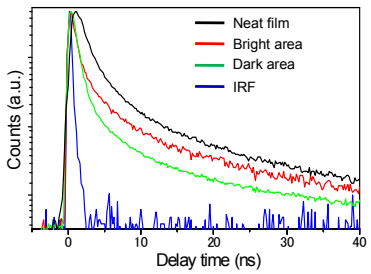

Fig. 6 Fluorescence decay curves observed from a DTA neat film (black) and a bright area (red) and dark area (green) in the fluorescence image of the OPV shown in Fig. 3(a) by a 405 nm excitation. The decay curve (blue) represents the instrument response function (IRF).

its high crystallinity.[20] Phase image of the active layer of the OPV is shown in Fig.S1 (a) in SI. The contrast of the phase image at the aggregates is different from other area. This observation strongly support that the aggregates have different film structure from other area, i.e., the aggregates probably consist of DTA crystalline structure. Therefore, the heterogeneity of the fluorescence image (Fig. 3a) was also due to the heterogeneity of DTA, as reflected in the difference in l in Eq.1. The bright areas in the fluorescence image (Fig. 3a) correspond to the aggregates of DTA. The fluorescence spectra observed from the bright and dark areas in the fluorescence image are shown in Fig. 5. Below 485 nm, the fluorescence spectra were cut off by a dichroic mirror that was inserted into the microscope to reflect the laser beam. The fluorescence peak at 510 nm was observed in both the bright and dark areas, although the signal-to-noise ratio in the spectrum measured in the dark area (Fig. 5b) was rather low. This peak was assigned to DTA.

These fluorescence spectra indicate that DTA was present within the entire active layer of the device, although the distribution was heterogeneous because of its tendency to aggregate. Figure 3 (b) corresponds to the fluorescence intensity distribution of $PC_{71}BM$ in the active layer of the device observed by a 640 nm excitation. In contrast to Fig. 3(a), the heterogeneity was not observed. The fluorescence spectrum observed by a 640 nm excitation is shown in Fig. 5 (c). The peak at 715 nm was characterized as representing $PC_{71}BM$, and this spectrum was observed at all locations within the device. The fluorescence image and the spectrum observed by a 640 nm excitation indicate that $PC_{71}BM$ was uniformly distributed over the entire area of the active layer. It is well known that the $PC_{71}BM$ forms aggregate with several tens of nanometer-size. Such aggregates were probably formed in our devices. However, as the sizes of the aggregates were much smaller than the diffraction limit of light, the uniform fluorescence image of $PC_{71}BM$ was observed. These results demonstrate that the spatial distribution of DTA and $PC_{71}BM$ in the active layer can be observed by varying the excitation and detection wavelengths. However, the ηED information cannot be clearly obtained from the fluorescence images due to the non-uniform distribution of DTA in the active layer, although the decrease in the fluorescence intensity of BHJ-OPV (Fig.3a) compared to the DTA neat film (Fig.3c) is probably caused by the charge transfer.

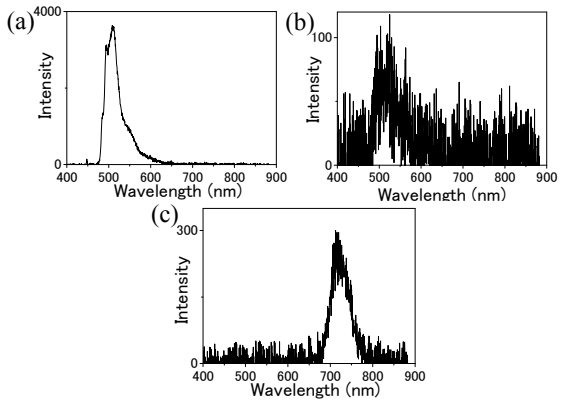

Fig. 5 Fluorescence spectra observed from the OPV consisting of DTA and $PC_{71}BM$. (a), (b) Fluorescence spectra observed from a bright area (a) and a dark area (b) in the fluorescence image shown in Fig. 3(a) by a 405 nm excitation. (c) Fluorescence spectrum observed from the fluorescence image shown in Fig. 3(c) by a 640 nm excitation.

The fluorescence lifetime measurements were conducted to evaluate the ηED of the OPVs. The fluorescence lifetime (τ) can be expressed as $\tau_{OPV}=1/(k_r + k_{nr} + k_{ED})$ for the OPV and as $\tau_{neat}=1/(k_r + k_{nr})$ for the neat film. Therefore, the contribution of k_{ED} can be estimated by comparing the lifetimes detected from the OPV and neat film. The fluorescence decay curves observed from the OPV and DTA neat film by a 405 nm excitation are shown in Fig. 6. The decay curves were analyzed by fitting with three exponential functions as follows:

$$I(t) = \alpha_1 exp(-t/\tau_1) + \alpha_2 exp(-t/\tau_2) + \alpha_3 exp(-t/\tau_3) \quad (3)$$

The fluorescence lifetimes (τ) and normalized amplitudes (α) obtained by the fitting are summarized in Table 2. The average lifetimes $<\tau>$ calculated by $\alpha_1\times\tau_1+\alpha_2\times\tau_2+\alpha_3\times\tau_3$ are also provided in this table. Figure 6 illustrates that the decay curves detected from the OPV were shorter than that detected from the DTA neat film. The shortened lifetime indicates the contribution of charge transfer in the device. The decay curve detected from a dark area was shorter than that detected from a bright area in the fluorescence image. In Table 2, the contribution of τ_1 in the decay curve detected from the dark area is greater than in the

Table 2. Fitting parameters for fluorescence decay curves.

		τ_1/ns	α_1	τ_2/ns	α_2	τ_3/ns	α_3	<τ>/ns
DTA	Neat film	0.8	0.57	2.3	0.36	9.2	0.07	1.93
	OPV Device Bright area	0.5	0.66	2.2	0.26	10.1	0.08	1.71
	Dark area	0.4	0.93	2.1	0.06	7.0	0.01	0.57
EH-DBTA	Neat film	0.5	0.64	1.9	0.31	5.5	0.05	1.18
	OPV Device	0.3	1.00	-	-	-	-	0.30

Fluorescence decay curves were fitted with a sum of three exponential functions, $I(t) = \alpha_1 exp(-t/\tau_1) + \alpha_2 exp(-t/\tau_2) + \alpha_3 exp(-t/\tau_3)$. The decay curve detected from the OPV device comprised of EH-DBTA and $PC_{71}BM$ was fitted with a single exponential function. τ and α represent the fluorescence lifetime and the normalized amplitude, respectively. <τ> is the averaged lifetime calculated by $\alpha_1 \times \tau_1 + \alpha_2 \times \tau_2 + \alpha_3 \times \tau_3$.

decay curve detected from the bright area. Hence, the average lifetime of the dark area is shorter than that of the bright area.

The difference in the decay curves observed in the bright and dark areas can be interpreted as follows. DTA formed aggregates in the bright areas in the fluorescence image, and the charge transfer only occurred at the surface of the aggregate, i.e., the excitons generated inside the aggregate did not contribute to the charge transfer. Therefore, the contribution of the short lifetime was lower and the fluorescence intensity was higher in the bright areas. In contrast, in the dark areas, the contribution of the charge transfer was higher than in the bright areas because the lifetime was shorter. However, the decay curves detected from both areas still included long lifetimes of 2.2 and 10.1 ns for the bright area and 2.1 and 7.0 ns for the dark area. If the charge transfer occurs efficiently, the decay curve should be consistent with the instrument response function (IRF).

The ηED was estimated by comparing the average lifetimes <τ> as follows. ηED is expressed as $\eta ED = k_{ED}/(k_r + k_{nr} + k_{ED})$. The average lifetimes of the neat film <τ_{neat}> and OPV <τ_{OPV}> are expressed as <τ_{neat}>=1/($k_r + k_{nr}$) and <τ_{OPV}> =1/($k_r + k_{nr} + k_{ED}$) , respectively; thus, k_{ED} = 1/<τ_{OPV}>−1/<τ_{neat}>, assuming that k_r and k_{nr} are constant in both the neat film and OPV. Therefore, ηED can be estimated using

$$\eta ED = 1 - <\tau_{OPV}>/<\tau_{neat}> \quad (4).$$

From Table 2, the average lifetimes in the bright area <τ_{OPV_B}> and dark area <τ_{OPV_D}> are 1.71 and 0.57 ns, respectively. Using these lifetimes, the ηED for the bright area and dark area can be estimated as 0.11 and 0.70, respectively. (ηED = 0.84 is the maximum value in this estimation because our IRF was 0.3 ns.) These values indicate that only 11% and 70% of the excitons generated in the DTA caused the charge transfer in the bright and dark areas, respectively. One reason for this low efficiency was the low compatibility of DTA with $PC_{71}BM$. As noted above, DTA tended to aggregate because of its high crystallinity. Therefore, there was a decrease in the interface between DTA and $PC_{71}BM$, where the charge transfer occurs.

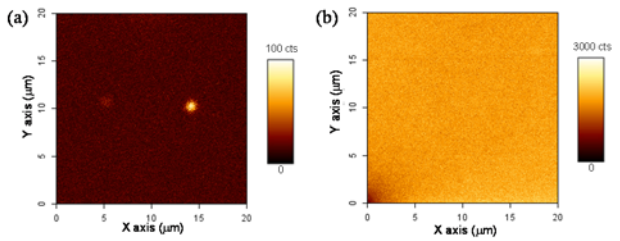

Fig. 7 Fluorescence images observed from an OPV consisting of EH-DBTA and $PC_{71}BM$ (a) and from an EH-DBTA neat film (b) by a 405 nm excitation with a 56 W/cm² intensity.

To improve the low compatibility, EH-DBTADK (Fig. 1b) which has branched alkyl-chains, was synthesized and used for device fabrication.[20] The fluorescence images observed from a BHJ-OPV fabricated using EH-DBTADK and $PC_{71}BM$ and from a neat film of EH-DBTA are shown in Fig. 7. In contrast to the DTA neat film, the heterogeneity of the fluorescence intensity was not observed in the image of the EH-DBTA neat film (Fig. 7b), indicating that EH-DBTA likely formed a uniform amorphous-like film because the crystallinity of EH-DBTA is lower than that of DTA. Therefore, the heterogeneity of the fluorescence intensity was not observed in the image of the OPV (Fig. 7a), although some fluorescence domains were observed. AFM images obtained from the OPV and neat film are shown in Fig. 8. Although small, broad peaks were observed in the AFM image, the peaks were considerably smaller than those in the AFM images of the DTA (Fig. 4). A comparison of the AFM images of the OPV with those of the neat film illustrates that the peaks were smaller in the OPV. In the phase AFM image shown in Fig.S1 (b), the heterogeneity of the image was not observed.

These results indicate that EH-DBTA could be miscible with $PC_{71}BM$ due to improved compatibility. We presume that EH-DBTA is not mixed with $PC_{71}BM$ at the molecular level, i.e., both compounds form the nanometer-sized aggregates in the active layer. If the EH-DBTA is mixed with $PC_{71}BM$ at the molecular level, the photovoltaic performance cannot be observed. As the sizes of aggregates are considerably smaller than the diffraction limit of light, therefore, the uniform fluorescence intensity was observed in the fluorescence images. The fluorescence decay curves obtained from the EH-DBTA

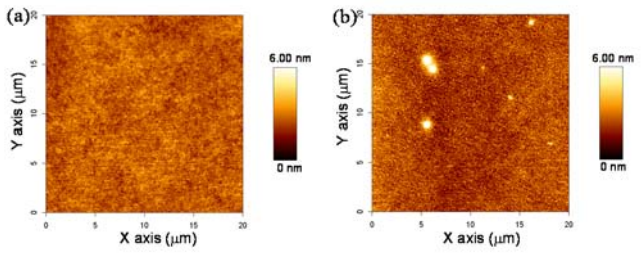

Fig. 8 AFM images obtained from the OPV consisting of EH-DBTA and $PC_{71}BM$ (a) and an EH-DBTA neat film (b).

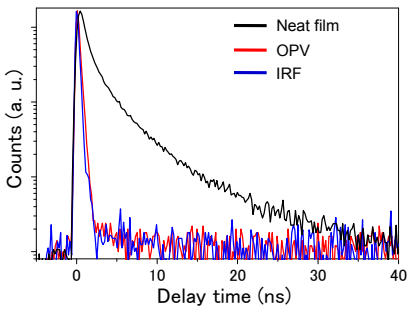

Fig. 9 Fluorescence decay curves observed from an EH-DBTA neat film (black) and the OPV (red) by a 405 nm excitation. The decay curve (blue) represents the instrument response function (IRF).

neat film and OPV are shown in Fig.9. The decay curve detected from the OPV was considerably shorter than that detected from the EH-DBTA neat film and nearly the same as the IRF. This result indicates that efficient charge transfer occurred in the OPV fabricated using EH-DBTADK and $PC_{71}BM$ and that the efficiency was higher than in the OPV comprised of DTA and $PC_{71}BM$. The fluorescence lifetimes (τ), normalized amplitudes (α), and average lifetimes $<\tau>$ obtained by the fitting are summarized in Table 2. An ηED of 0.75 was obtained using Eq.(1) with $<\tau_{OPV}>$=0.3 ns and $<\tau_{neat}>$=1.18 ns. The ηED of 0.75 reached the maximum value of our instrumental setup because the $<\tau_{OPV}>$ was the same as the IRF. Therefore, the ηED of the OPV device was over 75%. We can estimate the ηED more precisely using photo-detectors with high time resolution. The ηED was likely quite high, although it was not 100% because the fluorescence from EH-DBTA was still observed. These observations illustrate that efficient charge transfer occurred in the OPV device because EH-DBTA blended with $PC_{71}BM$ due to the low crystallinity of EH-DBTA.

As shown above, the ηED of the EH-DBTA:$PC_{71}BM$ device was considerably higher than that of the DTA: $PC_{71}BM$ device. This difference in ηEDs is related to the IQE and J_{SC} of the devices. Figure 2 indicates that the IQEs at 405 nm for the DTA:$PC_{71}BM$ and EH-DBTA:$PC_{71}BM$ devices were approximately 44% and 67%, respectively. From the fluorescence microspectroscopy measurements, the ηED at 405 nm for DTA:$PC_{71}BM$ was 11% in the bright area and 70% in the dark area, whereas the ηED for EH-DBTA:$PC_{71}BM$ was over 75%. The ηEDs were reduced to the values of the IQEs by the contributions of the ηCS and ηCC, and the IQDs decreased to the values of the EQEs by the contribution of ηA. For the BHJ-OPV considered here, the higher J_{SC} of the EH-DBTA:$PC_{71}BM$ device was attributed to the higher ηED due to the high compatibility between EH-DBTA and $PC_{71}BM$ using the high-sensitivity fluorescence microspectroscopy technique.

Conclusions

The spatially resolved ηED of BHJ-OPVs fabricated using photoprecusors and $PC_{71}BM$ was estimated by observing the fluorescence image, spectra, and lifetime using a confocal fluorescence microspectroscopy technique. For the BHJ-OPV composed of DTA and $PC_{71}BM$, a lower and more heterogeneous ηED was clearly observed even though the DTA and $PC_{71}BM$ existed over entire area of the active layer. This low, heterogeneous ηED was caused by the high crystallinity of DTA and the low compatibility of DTA with $PC_{71}BM$. Therefore, for the OPV consisting of EH-DBTA, which has a low crystallinity, and $PC_{71}BM$, the ηED was found to increase with increase in J_{SC} and PCE. However, PCE was quite low (0.85) in spite of the high ηED. As causes for the low PCE, the low efficiency of the carrier transportation from the BHJ layer to the electrodes (ηCC) can be considered. Recently, it was demonstrated that PCE can be increased to 2.83 by fabricating p-i-n (p:DTA neat film, i:BHJ of EH-DBTA and $PC_{71}BM$, n: $PC_{71}BM$ neat film) triple-layer architecture.[20] The present results indicate that the increase in the ηCC by fabricating p and n layers is a reason for the increase in the PCE of p-i-n OPV. In addition, the absorption efficiency (ηA) and the amount of subsequent carrier generation also increase because of the increase in the interfaces of p-i and i-n. Therefore, the increase in the PCE was observed by fabricating p-i-n architecture.

Acknowledgements

This work was partially supported by CREST from the Japan Science and Technology Agency (JST), a Grant-in-Aid for Scientific Research (Grant No. 26390023 for SM), a Grant-in-Aid for Scientific Research (Grant No. 25288092 for HY) from the Japan Society for the Promotion of Science (JSPS), the Green Photonics Project in NAIST sponsored by the Ministry of Education, Culture, Sports, Science and Technology (MEXT), Japan, and the program for promoting the enhancement of research universities in NAIST supported by MEXT.

Notes and references

[a] Department of Chemistry, Kwansei Gakuin University, 2-1 Gakuen, Sanda, Hyogo 669-1337, Japan. E-mail: masuo@kwansei.ac.jp; Tel&Fax: +81-79-565-7341

[b] Department of Organic Device Engineering, Yamagata University, Yonezawa 992-8510, Japan

[c] Graduate School of Materials Science, Nara Institute of Science and Technology, Ikoma 630-0192, Japan.

[d] CREST, Japan Science and Technology Agency (JST), Chiyoda-ku 102-0075, Japan.

† Electronic Supplementary Information (ESI) available: [details of instrumental setup, Phase AFM images of BHJ-OPVs].

1 Y. Y. Liang and L. P. Yu, *Acc. Chem. Res.* , 2010, **43**, 1227-1236.

2 P. M. Beaujuge and J. M. J. Frechet, *J. Am. Chem. Soc.*, 2011, **133**, 20009-20029.

3 D. Credgington and J. R. Durrant, *J. Phys. Chem. Lett.*, 2012, **3**, 1465-1478.

4 B. E. Hardin, H. J. Snaith and M. D. McGehee, *Nat. Photon.*, 2012, **6**, 162-169.

5 G. Li, R. Zhu and Y. Yang, *Nat. Photon.*, 2012, **6**, 153-161.

6 A. Mishra and P. Bauerle, *Angew. Chem. Int. Ed.*, 2012, **51**, 2020-2067.

7 H. J. Son, B. Carsten, I. H. Jung and L. P. Yu, *Energy Environ. Sci.*, 2012, **5**, 8158-8170.

8 H. X. Zhou, L. Q. Yang and W. You, *Macromolecules*, 2012, **45**, 607-632.
9 C. W. Tang, *Appl. Phys. Lett.*, 1986, **48**, 183.
10 N. S. Sariciftci, L. Smilowitz, A. J. Heeger and F. Wudl, *Synthetic Met*, 1993, **59**, 333-352.
11 N. S. Sariciftci, D. Braun, C. Zhang, V. I. Srdanov, A. J. Heeger, G. Stucky and F. Wudl, *Appl. Phys. Lett.*, 1993, **62**, 585.
12 J. J. M. Halls, C. A. Walsh, N. C. Greenham, E. A. Marseglia, R. H. Friend, S. C. Moratti and A. B. Holmes, *Nature*, 1995, **376**, 498-500.
13 G. Yu, J. Gao, J. C. Hummelen, F. Wudl and A. J. Heeger, *Science*, 1995, **270**, 1789-1791.
14 L. Dou, J. Gao, E. Richard, J. You, C. C. Chen, K. C. Cha, Y. He, G. Li and Y. Yang, *J. Am. Chem. Soc.*, 2012, **134**, 10071-10079.
15 Z. He, C. Zhong, X. Huang, W. Y. Wong, H. Wu, L. Chen, S. Su and Y. Cao, *Adv Mater*, 2011, **23**, 4636-4643.
16 J. You, L. Dou, K. Yoshimura, T. Kato, K. Ohya, T. Moriarty, K. Emery, C. C. Chen, J. Gao, G. Li and Y. Yang, *Nat. Commun.*, 2013, **4**, 1446.
17 M. Campoy-Quiles, T. Ferenczi, T. Agostinelli, P. G. Etchegoin, Y. Kim, T. D. Anthopoulos, P. N. Stavrinou, D. D. C. Bradley and J. Nelson, *Nat. Mater.*, 2008, **7**, 158-164.
18 Y. M. Nam, J. Huh and W. H. Jo, *J. Appl. Phys.*, 2011, **110**.114521.
19 Z. G. Xiao, Y. B. Yuan, B. Yang, J. VanDerslice, J. H. Chen, O. Dyck, G. Duscher and J. S. Huang, *Adv Mater*, 2014, **26**, 3068-3075.
20 Y. Yamaguchi, M. Suzuki, T. Motoyama, S. Sugii, C. Katagiri, K. Takahira, S. Ikeda, H. Yamada and K. Nakayama, *Sci. Rep.*, 2014, **4**, 7151.
21 L. Schmidt-Mende, A. Fechtenkotter, K. Mullen, E. Moons, R. H. Friend and J. D. MacKenzie, *Science*, 2001, **293**, 1119-1122.
22 P. Peumans, A. Yakimov and S. R. Forrest, *J. Appl. Phys.*, 2004, **95**, 2938-2938.
23 H. Benten, M. Ogawa, H. Ohkita and S. Ito, *Adv. Funct. Mater.*, 2008, **18**, 1563-1572.
24 A. Furube, Z. S. Wang, K. Sunahara, K. Hara, R. Katoh and M. Tachiya, *J. Am. Chem. Soc.*, 2010, **132**, 6614-6615.
25 J. Guo, H. Ohkita, S. Yokoya, H. Benten and S. Ito, *J. Am. Chem. Soc.*, 2010, **132**, 9631-9637.
26 X. F. Wang, L. Wang, Z. Q. Wang, Y. W. Wang, N. Tamai, Z. R. Hong and J. Kido, *J. Phys. Chem. C*, 2013, **117**, 804-811.
27 S. Gelinas, A. Rao, A. Kumar, S. L. Smith, A. W. Chin, J. Clark, T. S. van der Poll, G. C. Bazan and R. H. Friend, *Science*, 2014, **343**, 512-516.
28 Y. Q. Gao, T. P. Martin, A. K. Thomas and J. K. Grey, *J. Phys. Chem. Lett.*, 2010, **1**, 178-182.
29 J. H. Huang, F. C. Chien, P. L. Chen, K. C. Ho and C. W. Chu, *Anal. Chem.*, 2010, **82**, 1669-1673.
30 D. P. Ostrowski, M. S. Glaz, B. W. Goodfellow, V. A. Akhavan, M. G. Panthani, B. A. Korgel and D. A. V. Bout, *Small*, 2010, **6**, 2832-2836.
31 T. J. K. Brenner and C. R. McNeill, *J. Phys. Chem. C*, 2011, **115**, 19364-19370.
32 X. T. Hao, L. M. Hirvonen and T. A. Smith, *Methods Appl. Fluoresc.*, 2013, **1**, 015004.
33 H. Yamada, E. Kawamura, S. Sakamoto, Y. Yamashita, T. Okujima, H. Uno and N. Ono, *Tetrahedron Lett.*, 2006, **47**, 7501-7504.
34 T. Motoyama, T. Kiyota, H. Yamada and K. Nakayama, *Sol. Energy Mater. Sol. Cells*, 2013, **114**, 156-160.
35 T. Motoyama, S. Sugii, S. Ikeda, Y. Yamaguchi, H. Yamada and K. Nakayama, *Jpn. J. Appl. Phys.*, 2014, **53**, 01AB02.
36 M. Maus, M. Cotlet, J. Hofkens, T. Gensch, F. C. De Schryver, J. Schaffer and C. A. M. Seidel, *Anal. Chem.*, 2001, **73**, 2078-2086.

Graphical Abstract

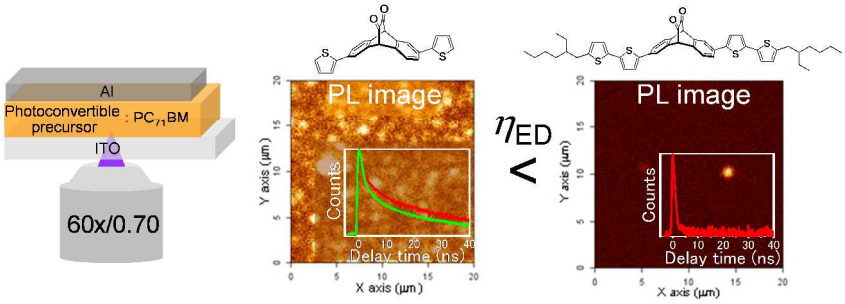

Evaluation of the charge transfer efficiency of organic thin-film photovoltaic devices using fluorescence microspectroscopy